01 Nov 2018

Column-Footing Connection Evaluation of Hollow-Core Composite Bridge Columns

Mohanad M. Abdulazeez

Mohamed ElGawady
Missouri University of Science and Technology, elgawadym@mst.edu

Recommended Citation

M. M. Abdulazeez and M. ElGawady, "Column-Footing Connection Evaluation of Hollow-Core Composite Bridge Columns," *ACI Symposium Publication*, vol. 327, pp. 39.1-39.14, American Concrete Institute (ACI), Nov 2018.

Column-Footing Connection Evaluation of Hollow-Core Composite Bridge Columns

Mohanad M. Abdulazeez, Ahmed Gheni, Omar I. Abdelkarim, and Mohamed A. ElGawady

Synopsis: This paper presents the seismic behavior of two large-scale hollow-core fiber-reinforced polymer-concrete-steel (HC-FCS) precast columns having two different footing connections. The precast HC-FCS column consists of a concrete shell sandwiched between an outer fiber-reinforced polymer (FRP) tube and an inner steel tube. The steel tube was embedded 635 mm (25 inches) into a reinforced concrete footing, while the outer FRP tube confined the concrete shell only i.e. it was truncated at the top surface of the footing. One connection included embedding the steel tube into the footing. The other one included using a corrugated steel pipe (CSP) embedded into the concrete footing outside the steel tube to achieve better confinement. This study showed that the connection including the CSP is deemed satisfactory and was able to develop the plastic flexural capacity of the HC-FCS column providing good ductility and energy dissipation compared with the other connection type.

Keywords: Column-Footing Connection, Precast Columns, Composite Columns, Fiber Reinforced Polymer (FRP), Corrugated Steel Pipe, Seismic Loading, Hollow Core.

ACI member **Mohamed ElGawady** is Benavides Associate Professor in the Department of Civil, Architectural & Environmental Engineering at Missouri University of Science and Technology, Rolla, MO. He is an Associate editor of the Journal of Bridge Engineering, ASCE, Chair of the ACI-ASCE Committee 441, Chair of the ACI341A, and Secretary of the Prestressed Masonry Committee, TMS 402/602.

ACI member **Omar I. Abdelkarim** is a postdoctoral fellow at the Université de Sherbrooke.

ACI student member **Ahmed Gheni** is a PhD candidate in the Department of Civil, Architectural & Environmental Engineering at Missouri University of Science and Technology, Rolla, MO 65409.

ACI student member **Mohanad M. Abdulazeez** is a Graduate Student and PhD candidate in the Department of Civil, Architectural & Environmental Engineering at Missouri University of Science and Technology, Rolla, MO 65409.

INTRODUCTION

The most common type of bridge column construction in the United States is cast-in-place (CIP). However, CIP requires long on-site construction time, labor-intensive resources, and long-term closure, which may result in traffic congestion [1]. Therefore, there is currently a momentum for developing accelerated bridge construction (ABC) methods to address these challenges. ABC reduces traffic disruptions and life-cycle costs and improves construction quality and safety, resulting in more sustainable development [2]. One technique to accelerate bridge construction is to use precast bridge columns. Several regions around the world are susceptible to earthquakes. Hence, the developed precast column component needs to display good seismic performance.

A good candidate for precast columns is concrete-filled tube, which consists of a hollow tube made out of steel or fiber-reinforced polymer filled with concrete. Another candidate for precast columns is the hollow-core steel-concrete-steel (HC-SCS) columns consisting of two generally concentric tubes with concrete shell between them [3-10]. The inner tube is empty, i.e., unfilled with concrete, to reduce the weight of the column. HC-SCS columns can also be cast-in-place, with the outer and inner tubes acting as stay-in-place formwork. The concrete infill is confined by both tubes, resulting in high concrete confinement and column ductility [10]. All of the research mentioned showed the superior seismic and axial capacity of HC-SCS columns. Recently, Teng et al. (2004) replaced the outer tube in the HC-SCS column with fiber reinforced polymer (FRP) tube creating HC-FCS column. FRP tube has higher strength-to-weight ratio compared to that of the steel tube. Furthermore, FRP is more corrosion resistance compared with steel. The performance of HC-FCS columns under axial, axial-flexural, and vehicle impact were investigated and showed superior performance compared to conventional reinforced concrete columns [4, 9, 11-19]

Several regions around the world are susceptible to earth-quakes where large ductility demands are imposed on bridge columns. The design and the construction of a column-footing connection is crucial for precast columns to meet the ductility demands. The connection must be effective to develop the ultimate strength and displacement of the column without significant slip; the connection needs also to be simple and economic to be used for ABC. Different types of connections that were proposed in the literature for concrete filled steel tube (CFST) columns, including welded and bolted steel plate, embeded base and rebars, and embeded structural steel connections were used for precast column-footing connections [20-23]. These solutions were either insufficient or slowed the construction.

Simple socket connections were also developed in the past for CFST [24]. For cast-in-place footing, a precast column is inserted into the steel cage footing; then, the footing is cast. In the case of a precast footing, the concrete footing is cast first with a socket of a larger diameter than the column's diameter and the required embedment length; then, the column is inserted into the socket, followed by grouting the gap between the column and sides of the socket. Experimental investigations have revealed that socket connections of this type have three distinct potential failure modes depending on the embedment length [25-27]. Pullout failure occurs when the embedment length is not sufficient. Punching shear failure occurs with a shallow footing depth below the CFST column. Otherwise, the connection may develop the full strength and displacement capacity of the column with sufficient embedment length; hence, the failure occurs in the column.

Recently, Abdelkarim et al. [15] tested a 0.4-scale HC-FCS column, F4-24-E344, under constant axial load and lateral cyclic load. The column reached a drift of 11.6 %. The test was terminated due to pull out failure of the footing without visual damage to the column. More details about that test will be given later in this paper.

RESEARCH SIGNIFICANCE

The current study aims at improving the column-footing connection. In particular, the main objectives of this study are to investigate: (1) the performance of socket connection having an embedded corrugated steel pipe (CSP) into the footing for precast columns; (2) whether embedded corrugated steel pipe (CSP) into the footing will compensate for the insufficient embedment length of the steel tube.

EXPERIMENTAL PROGRAM

In this study, the column F4-24-E344 originally tested by Abdelkarim et al. [15] was inserted into a newly constructed footing including a CSP to form column F4-24-E344-RS (Fig. 1) and was retested under constant axial load and lateral cyclic load similar to those used by Abdelkarim et al. [15]. F4-24-E344-RS column had a circular cross-section with an outer diameter of 610 mm (24 inches) and a clear height of 2,032 mm (80 inches) [Fig. 1 (c)]. The lateral load was applied at a height of 2413 mm (95 inches) with a shear span-to-depth ratio of approximately 4.0. The column consisted of an outer filament-wound glass fiber (GFRP) tube with a thickness of 9.5 mm (0.375 inch) and an inner steel tube having an outer diameter of 406 mm (16 inches) and a thickness of 12.7 mm (0.50 inch). A concrete shell having a thickness of 102 mm (4 inches) was used between the steel and FRP tubes. F4-24-E344-RS had an embedment steel tube length of 635 mm (25 inches) corresponding to 1.6 D_i.

The columns' label used in their experimental work consisted of three segments. The first segment is the letter F, referring to flexural testing followed by the column's height-to-outer diameter ratio of 4. The second segment refers to the column's outer diameter (D_o). The third segment refers to the glass fiber (GFRP) matrix, the steel, and the concrete shell, where E has been used for resin type epoxy; this is followed by the GFRP thickness in 3.175 mm (1/8 inch), steel thickness in 3.175 mm (1/8 inch), and concrete wall thickness in 25.4 mm (1 inch). The last letters "RS" refer to recess connection using CSP that was implemented in this column.

To determine the diameter and depth of the embedded CSP, Abdelkarim et al. [15] carried out finite element analysis FEA study and following earlier work on CFST to derive equation (1)

$$\frac{DD_{ii}\,tt_{ss}FF_{uu}}{\left(DD_{oo}+DD_{ii}\right)^{2}+DD_{oo}\,ll_{ee}} \leq 3.3\sqrt{ff'_{cc,FFFF}} \qquad (1)$$

where D_i is the steel tube outer diameter (inch), t_s is the steel tube thickness (inch), F_u is the ultimate stress of steel tube (ksi), D_o is the outer diameter of an annual ring welded with the bottom of steel tube or the outer diameter of the corrugated steel pipe (inch), l_e is the development length (inch), and ff'_{ccFFFF} is the unconfined cylindrical compressive strength of the concrete footing (ksi).

The concrete footing that was used in this study had a length x width x depth of 1,524 mm x 1,220 mm x 864 mm (60 inches x 48 inches x 34 inches) with bottom reinforcements of 7#8, top reinforcements of 6#8, and shear reinforcement of #4 bar at 63.5 mm (2.5 inches) which is similar to the footing used by Abdelkarim et al. [15]. The steel cage of the footing was installed into the formwork. A 914 mm (36 inches) outer diameter (D_{csp}) corrugated steel pipe (CSP) having a height of 635 mm (25 inches) and thickness of 4 mm (0.16 inch) was placed inside the footing. The diameter of the CSP was determined using equation (1). The CSP was embedded with its full height of 635 mm (25 inches), similar to the inner steel tube embedded length, into the footing. Then, four small spots were cut atop of the CSP, allowing the top layer of footing reinforcement bars to sit on the top of the CSP. To this end, it would be possible to cast the footing, insert the column, and pour grout in-between the 914 mm (36 inches) diameter CSP and the 406 mm (16 inches) diameter inner steel tube of the column. However, this would require a significant amount of grout. To avoid this large amount of grout, a temporary 508 mm (20 inches) diameter CSP was placed into the footing inside the main CSP before casting the footing [Fig. 1 (b)].

Once the CSPs were installed, the footing was cast including the space between the two CSP's [Fig. 1 (d)]. After one day, the temporary CSP was removed, leaving a corrugated concrete surface [Fig. 1 (e)]. For field implementation, both CSPs would be kept in place. However, during, the current work the inner CSP was removed as it was used for other projects. Fourteen days after casting the footing, the column was erected with an embedment length of 635 mm (25 inches). The 50.8 mm (2 inches) left between the corrugated concrete surface and the column inner steel tube surface was filled with high-strength flowable grout. One inlet pipe and two outlet pipes were used in order to ensure filling all the space around the column inside the footing [Fig. 1 (e)].

Grout was placed using a 38.1 (1.5 inch) clear flex PVC pipe and funnel, located 3,048 mm (10 ft high) above the level of the footing top surface, using the gravity pipe method. The grout was continuously placed through the funnel until it came out of the outlet pipes in order to ensure complete filling of the gap between the column inner steel pipe and the surrounding concrete surface. The final F4-24-E344-RS column layout is shown in [Fig. 1 (b)].

The mechanical properties of the steel tube and rebar are summarized in Table 1. The rebar properties are based on the manufacturer's data sheet while the steel tube properties were determined through tensile steel-coupon testing according to ASTM A 1067. The concrete and grout mix designs are shown in Tables 2 and 3, respectively. Pea gravel with maximum aggregate size of 9.5 mm (3/8 inch) was used for concrete mixtures. Table 4 summarizes the unconfined concrete strength for the footing, column, and the high strength grout. The material properties of the GFRP tube are presented in Table 5.

Table 1 — Steel properties of the rebars and steel tubes

	Elastic modulus [GPa (ksi)]	Yield stress [MPa (ksi)]	Ultimate stress [MPa (ksi)]	Ultimate strain ε_u, [mm/mm (in/in)]
Steel rebar	200 (29,000)	413 (60)	620 (90)	0.08
Steel tube	200 (29,000)	324 (47)	483 (70)	0.19

Table 2 — Concrete mixture proportions

w/c	Cement [kg/m^3 (lb/yd^3)]	Fly Ash [kg/m^3 (lb/yd^3)]	Water [kg/m^3 (lb/yd^3)]	Fine Aggregate [kg/m^3 (lb/yd^3)]	Coarse Aggregate [kg/m^3 (lb/yd^3)]
0.5	350 (590)	101 (170)	225 (380)	848 (1,430)	848 (1,430)

Table 3 — High strength grout mixture proportions

w/c	Cement Type III [kg/m^3 (lb/yd^3)]	Silica Fume [kg/m^3 (lb/yd^3)]	Water [kg/m^3 (lb/yd^3)]	Fine Aggregate [kg/m^3 (lb/yd^3)]	Masonry Sand [kg/m^3 (lb/yd^3)]	HRWR [kg/m^3 (lb/yd^3)]
0.21	1074 (1809)	72 (121)	244 (412)	727 (1225)	318 (536)	82 (139)

Table 4 — Unconfined concrete strength of the columns and the footings

	F4-24-E344 [28]		F4-24-E324-RS	
	Column	Footing	Footing	HS-Grout
f'_c at 28 days [MPa (ksi)]	40 (5.8)	56 (8.1)	55 (7.9)	64 (9.3)
f'_c (day of test) [MPa (ksi)]	54 (7.8)	59 (8.6)	56 (8.1)	66.5 (9.6)

Table 5 — FRP tubes properties

Elastic modulus [GPa (ksi)]	Hoop elastic Modulus [GPa (ksi)]	Axial ultimate stress [MPa (ksi)]	Hoop rupture stress [MPa (ksi)]
4.7 (677)	21 (3,020)	83 (12.15)	277 (40.15)

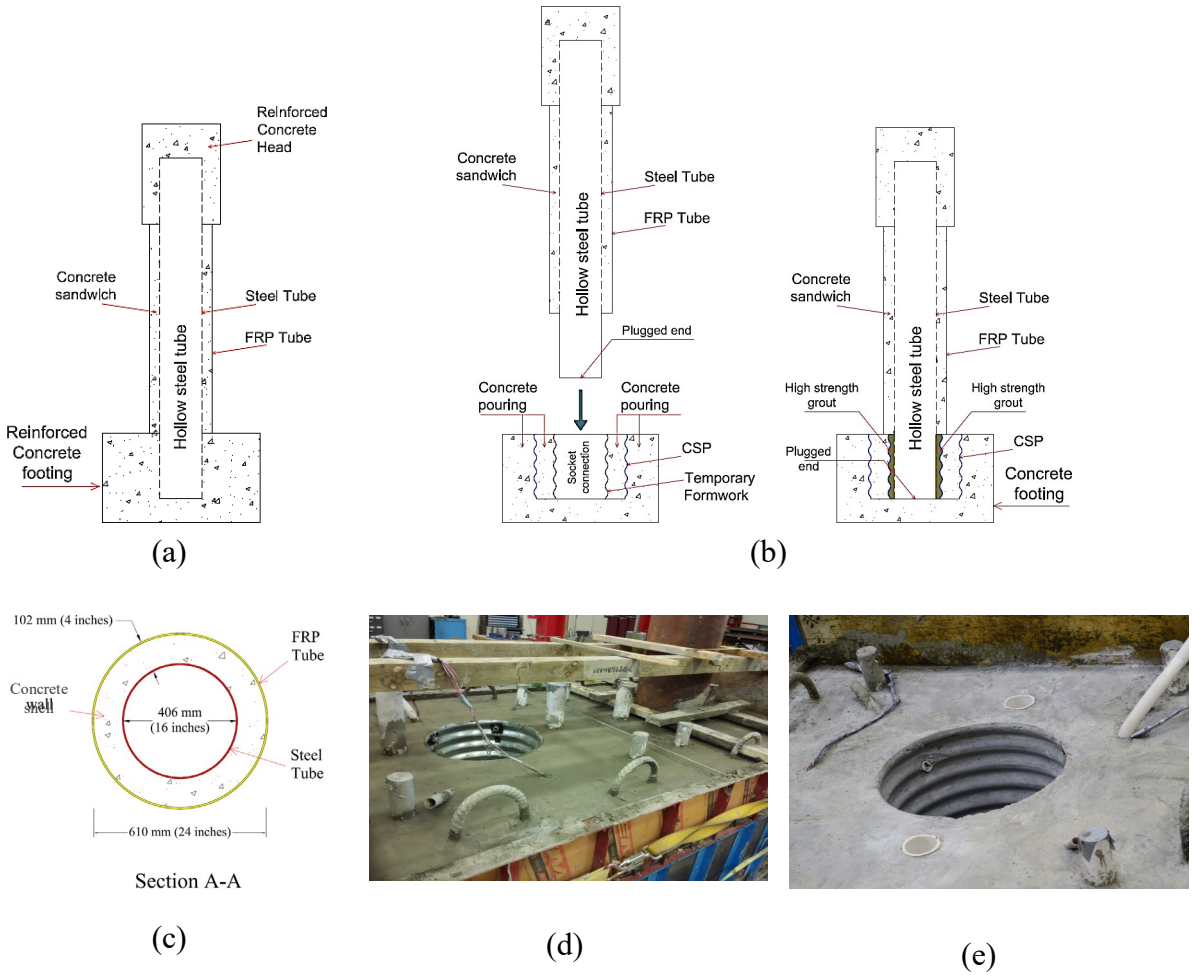

Figure 1— General arrangement of the column-footing connection for column F4-24-E344-RS: (a) without CSP [15], (b) construction sequence with CSP, (c) column cross-section, (d) after pouring of the concrete footing, (e) after removing the temporary CSP form

EXPERIMENTAL SETUP AND INSTRUMENTATION

Sixteen linear-variable-displacement-transducers (LVDT) and string potentiometers (SP) were used to measure displacement along column F4-24-E324-RS [Fig. 2 (a)]. Four LVDTs were mounted on each of the north and south faces for the vertical displacement measurements at the potential plastic hinge region. Two more LVDTs were used to measure the uplift and sliding of the footing during the test.

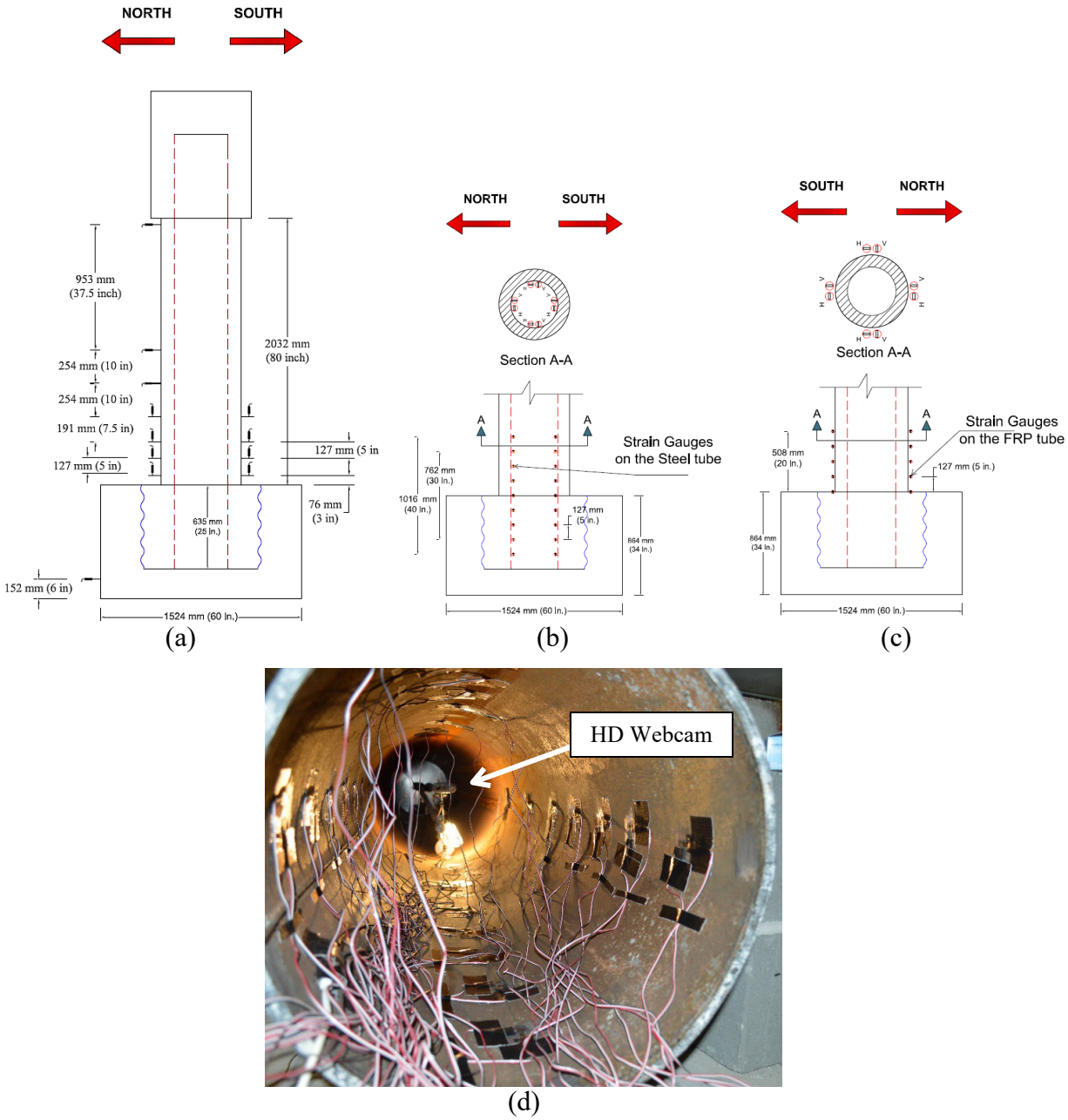

Figure 2 — Instrumentation layout of the tested column F4-24-E344-RS (a) LVDTs installation; (b) Strain gauges mounted on GFRP tube 127 mm (5 inches) apart; (c) Strain gauges mounted on Steel tube 127 mm (5 inches) apart; and (d) Webcam directed downward inside the steel tube before erecting the column

Forty strain gauges were installed on the FRP tube at five levels with 127 mm (5 inches) spacing. Four horizontal and four vertical strain gauges were installed at each level [Fig. 3 (b)]. Fifty-six strain gauges were installed inside the steel tube at seven levels with spacing of 127 mm (5 inches) [Figs. 3 (c) and (d)]. Four horizontal and four vertical strain gauges were installed at each level. A high definition webcam was hung inside the steel tube vertically at 635 mm (25 inches) from the top of the footing level to broadcast buckling of the steel tube and any internal damage [Fig. 3 (d)].

LOADING PROTOCOL AND TEST SETUP

The axial load capacity P_o of an equivalent RC-column with the same diameter 610 mm (24 inches) and 1% longitudinal reinforcement ratio was calculated using equation (2) [32]:

$$\mathbb{P}_{oo} = AA_{ss}\,\mathbb{F}_{yy} + 0.85\,(AA_{cc} - AA_{ss})\,ff'cc \quad (2)$$

where AA_{ss} = the cross-sectional area of the longitudinal steel reinforcements, AA_{cc} = the cross sectional area of the concrete column, $\mathbb{F}_{yy}$ = the yield stress of the longitudinal steel reinforcement, and $ff'cc$ = the cylindrical concrete's unconfined compressive stress.

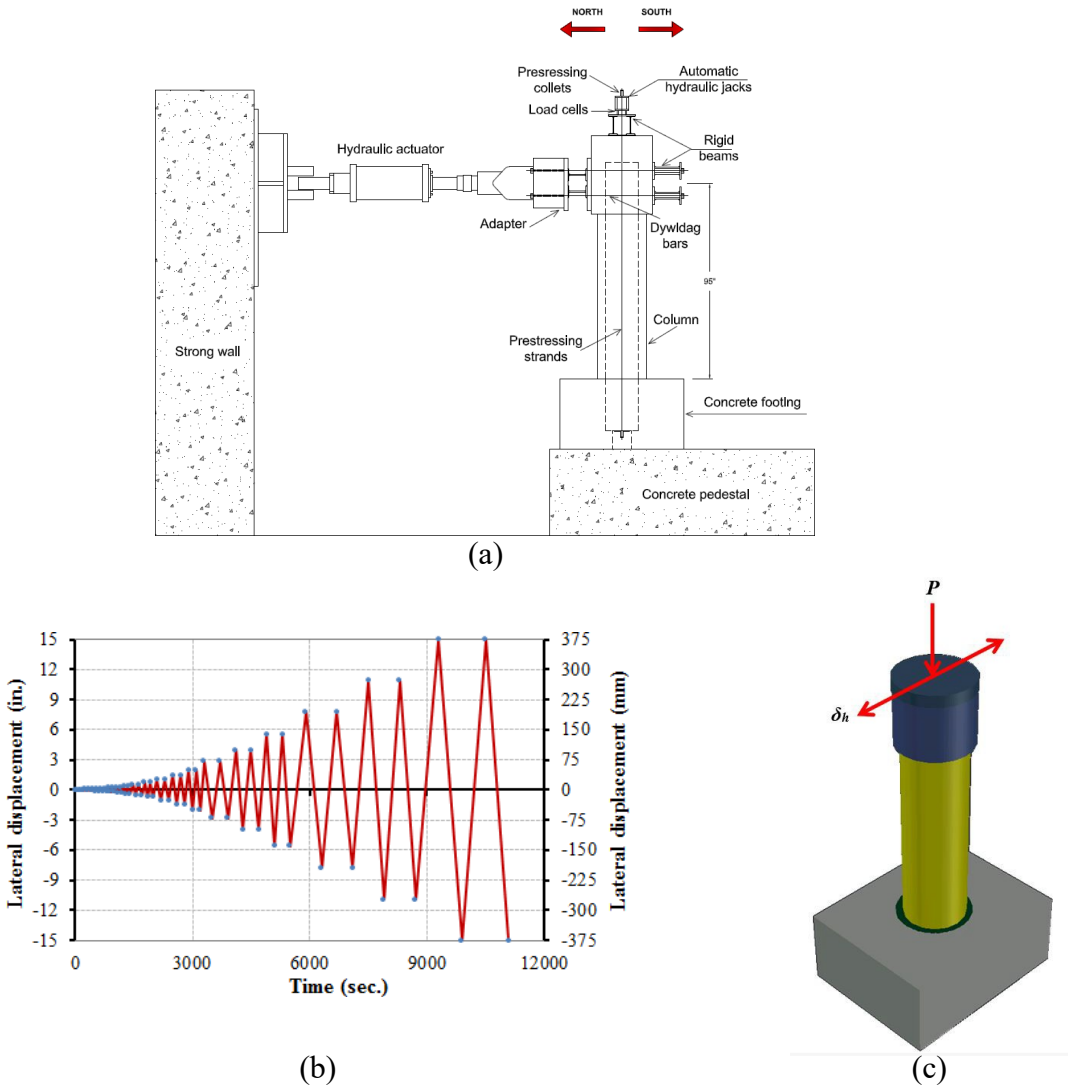

Figure 3 — (a) Layout of the test setup (b) Lateral displacement loading regime; and (c) 3D view

Constant axial load, P, of 489.3 kN (110 kips) corresponding to 5% of the calculated P_o was applied to the column using three external prestressing strands on each of the west and east sides of the column [Fig. 3 (a)]. The axial load represented 5% of the nominal axial capacity (P_o) of a conventional solid RC column of the same outer diameter in compression as the investigated columns with 1% of longitudinal reinforcement. The prestressing force was applied using two servo-controlled jacks to keep the prestressing force constant during the test. The prestressing strands were

supported by a rigid steel beam atop the column and the column's footing. After applying the axial load, static cyclic lateral load was applied in a displacement control using two hydraulic actuators connected to the column loading stub [Fig. 3 (a)]. The loading regime is based on the recommendations of FEMA 2007. Two cycles were performed for each displacement amplitude. Figure 3 (b) shows the loading regime of the cyclic lateral displacement.

RESULTS AND DISCUSSIONS

Abdelkarim et al. [15] investigated two columns, namely F4-24-E324 and F4-24-E344. Each column had a socket connection with an embedment length of 635 mm (25 inches) corresponding to 1.6 D_i. Two distinct modes of failure occurred for the same steel tube diameter and embedment length, depending on the steel tube thickness. For column F4-24-E324 with a relatively thin steel tube of 6.35 mm (0.25 inch), the socket connection was able to develop the full capacity of the column and the steel tube yielded with no pinching in the hysteretic curve [Fig. 4 (a)]. The column's footing did not suffer any significant visual damage. For column F4-24-E344 with a retaively thick steel tube of 12.7 mm (0.5 inch), the socket connection was not able to develop the full capcity of the column and pullout failure occurred with severe pinching in the hysteretic curves. The column's footing suffered severe damage due to the pullout as well.

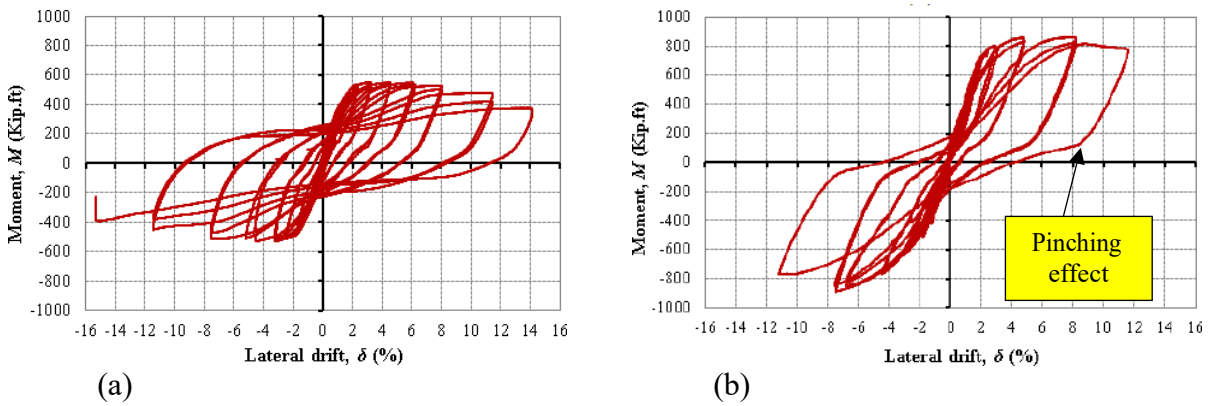

Figure 4— Moment vs. lateral drift for column: (a) F4-24-E324 [15] , and (b) F4-24-E344 [15]

During this study, the column F4-24-E344 was inserted into a newly constructed footing including the CSP to form column F4-24-E344-RS and was retested. The moment versus lateral drift plot of column F4-24-E344-RS is shown in Figure 5. The lateral drift ($\delta\delta$) was calculated by dividing the lateral displacement measured from the actuators' displacement transducers by the shear span of 2,413 mm (95 inches). The moment at the base of the column was obtained by multiplying the force measured by the actuators' loading cells by the column's shear span. Figure 5 and Table 6 show that using CSP significantly improved the performance of F4-24-E344-RS by displaying 10% higher flexural strength and 20% higher lateral drift compared to column F4-24-E344.The average moment capacity of the column was 1,310 kN.m (966 kip.ft) which occurred at a lateral drift of 10.7%. Gradual stiffness degradation occurred beyond that until the end of the test. Figure 6 shows steel tube buckling captured through the camera inside the steel tube at different lateral drifts. At a lateral drift of 14.5%, the FRP ruptured at the south direction (Fig. 7). Cycling continued toward the north direction untill a lateral drift of 15.1% when the test was stopped because the actuator had reached its displacement capacity limit.

Figure 5 (b) illustrates a comparison between the cyclic response of the two columns F4-24-E344-RS and F4-24-E344. As shown in the figure, the prevention of the pullout failure resulted in fat hysteretic loops resulting in high energy dissipation, which is an essential characteristic for seismic applications.The existence of CSP controlled the splitting "zipping" cracking mechanism and dilation of the concrete in the footing, and hence reduced concrete cracking delaying the pullout of the column. Hence, the CSP plays a role of confinement in the footing.

Figures [5 (c) and (d)] shows the backbone curves of the two columns. Also, shown on the figures are the idealized elasto-plastic curves developed following [29]. The idealized curves were used to calculate the displacement ductility of the columns. As shown in the figure, the columns reached displacement ductility values of 6.80 and 7.20 for columns F4-24-E344 [15] and F4-24-E344-RS, respectively. Both values exceed the maximum anticipated

displacement ductility demand of 5 imposed by AASHTO Guide Specifications for LRFD Seismic Bridge Design on single bridge column bent [31]. It also exceeds the minimum requirements displacement ductility of 3 imposed by Caltrans [30].

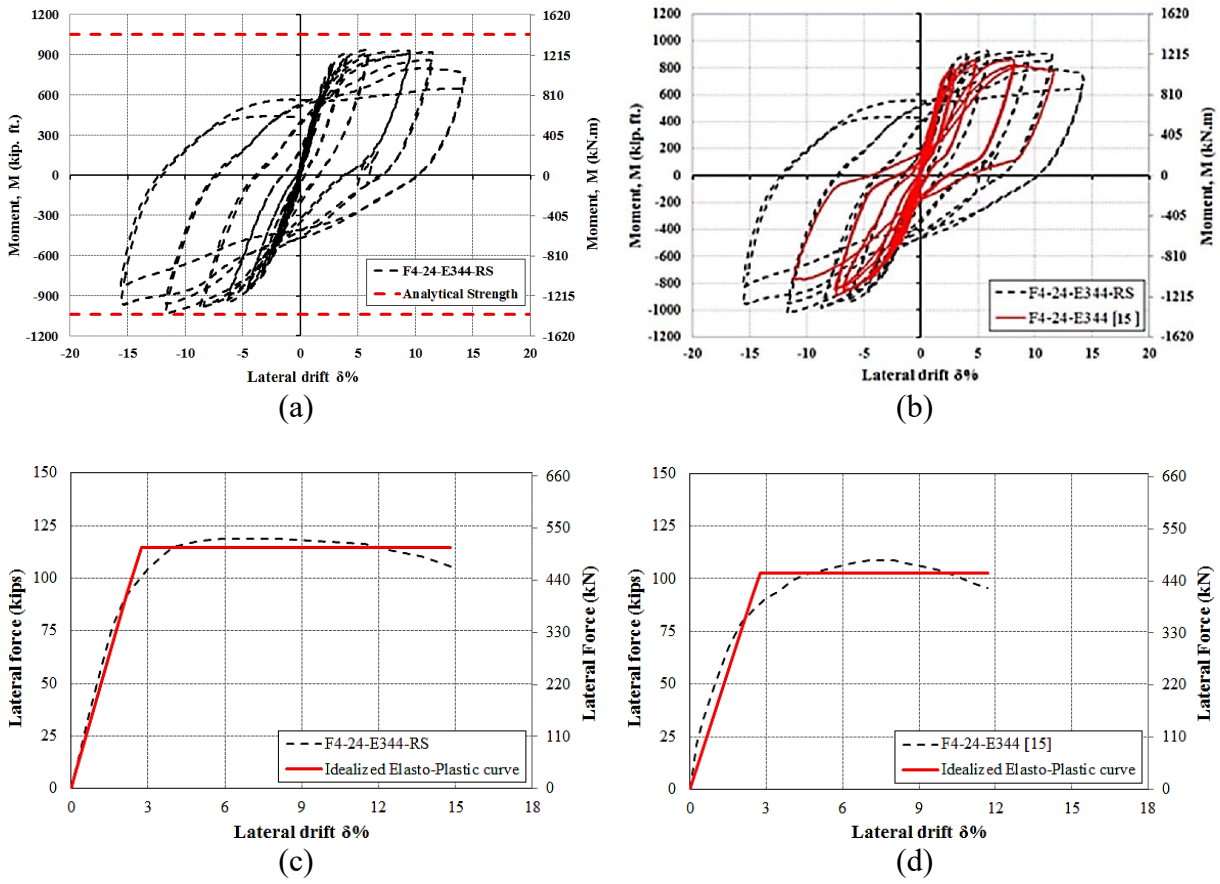

Figure 5 — Moment vs. lateral drift (a) for column F4-24-E344-RS; (b) for columns F4-24-E344-RS and F4-24-E344 [15]; (c) Idealized elasto-plastic curve for column F4-24-E344-RS; and (d) Idealized elasto-plastic curve for column F4-24-E344 [15]

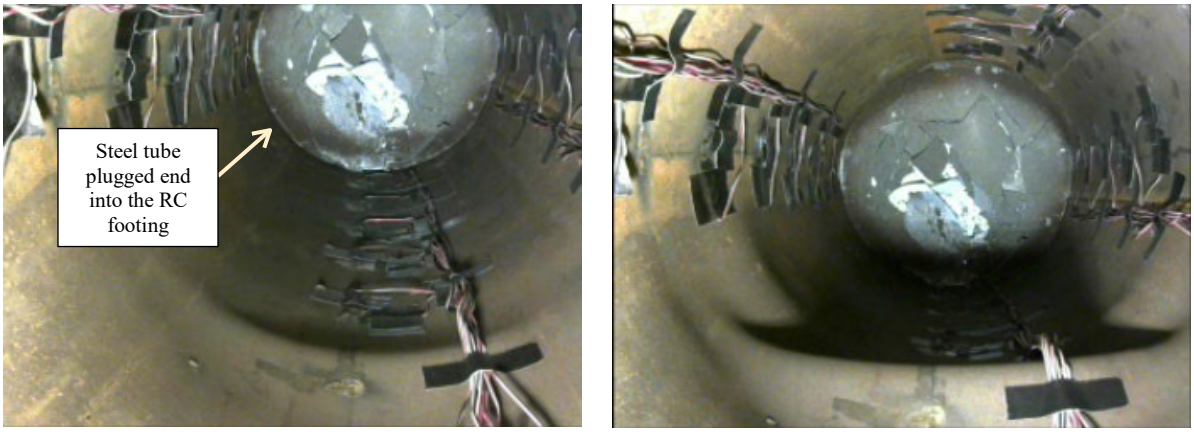

Figure 6 — Local buckling of the steel tube of the column F4-24-E344-RS at lateral drifts of (a) 11.3%, and (b)14%

Figure 7— FRP rupture of the column F4-24-E344-RS at a lateral drift of 14.5%

Using CSP was able to superseeded severe damage to the footing og column F4-24-E344-RS. Figure 8 shows a comparison between column F4-24-E344-RS and column F4-24-E344 [15] footings. The footing of column F4-24-E344-RS displayed cracks having widths ranging from 0.15 to 0.20 mm (0.006 to 0.008 inch) which is within the ACI 224R-01 limits for a structure in contact with soil. However, the footing of column F4-24-E344 [15] suffered severe damage due to pullout indicating that the existence of the CSP-precluded pullout failure, crack propagation, and footing damage.

Figure 9 illustrates the cumulative energy dissipation-lateral drift relation for the columns F4-24-E344 [15] and F4-24-E344-RS. The energy dissipation at each lateral drift was determined as the area enclosed in the hysteretic loop of the first cycle at this drift level. Dissipating greater hysteretic energy increases the ability of a structure to sustain higher magnitude earthquakes and is an essential characteristic for seismic applications. As shown in the figure, both columns had almost the same energy dissipation until lateral drift of approximately 5%. Beyond this drift, column F4-24-E344 [15] displayed severe pinching and limited energy dissipation due to the steel tube pullout. At a drift of 11.6% when the column F4-24-E344 [15] failed, column F4-24-E344-RS dissipated 64% greater energy. Furthermore, column F4-24-E344-RS was able to sustain the applied cyclic loads until a drift of 14.5%. At failure, column F4-24-E344-RS dissipated 270% greater energy than column F4-24-E344 [15], indicating better seismic performance.

(a) (b)

Figure 8 — Footing (a) Hairline cracks in the footing of column F4-24-E344-RS at lateral drift 14.5%, and (b) severe damage in the footing of column F4-24-E344 [15] at lateral drift 11.6%

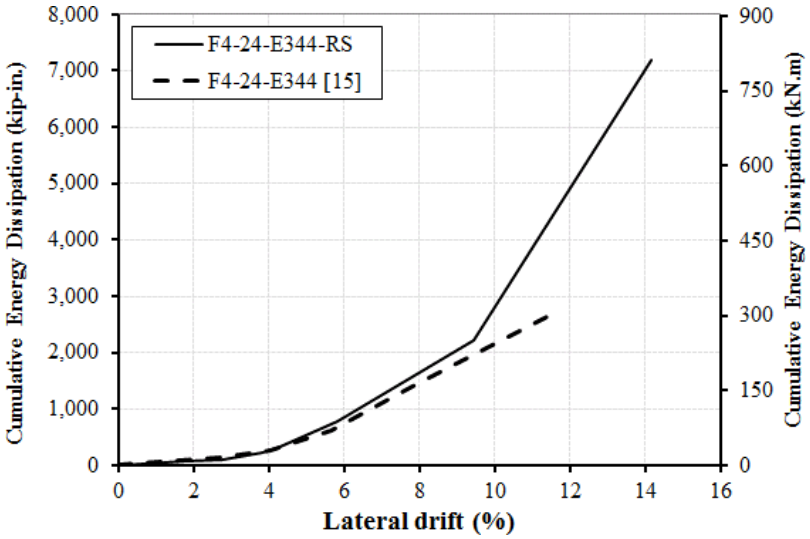

Figure 9 — Cumulative energy dissipation vs. lateral drift for columns F4-24-E344-RS and F4-24 E344 [15]

Table 6— Summary of the results of both HC-FCS column

Tested Column	Moment capacity [kN.m (kip. ft.)]	Lateral drift at failure (%)	Mode of failure
F4-24-E344 [15]	1,186 (875)	11.6%	Sever pullout and Footing crushing
F4-24-E344-RS	1,310 (966)	14.5%	Steel tube local buckling, concrete shell crushing, and FRP rupture

FLEXURAL STRENGTH OF HC-FCS COLUMNS

The flexural strength of HC-FCS columns can be calculated used Bernoulli–Navier's assumptions assuming elasto-plastic model for the steel and linear elastic model for the FRP. The confinement model developed in [29] was used for concrete shell in the column. The analytical model is described below in the manuscript. Using this approach, the strengths of the columns were calculated as 1,424 kN.m (1,050 kip.ft) for columns F4-24-E344 and F4-24-E344-RS, respectively. Hence, as shown in Figure (5 (b)), the model underestimated the flexural strength by 17% and 10.7% for columns F4-24-E344 and F4-24-E344-RS, respectively. The underestimation is much higher for column F4-24-E344 due to the early slippage that took place early during testing. While it was found to be less for column F4-24-E344 equal to 10.7% due to the existence of the CSP which reduced the slip of the steel tube out of the footing and thereby higher flexural capacity was achieved.

The following analytical model was used to predict the strength of the tested column [15].

1- Compute the sectors' polar angles ($\theta\theta_1, \theta\theta_2 \& \theta\theta_3$)

$$\theta\theta_1 = \frac{\alpha\alpha_1}{(nn)}, \theta\theta_2 = \frac{\alpha\alpha_2}{(nn)} \& \theta\theta_3 = \frac{\alpha\alpha_3}{(nn)} \quad (3)$$

where n is the number of strip segments = 100 in this study

2- Compute the strain in each strip segment

$$\varepsilon\varepsilon_{cc1nn} = \frac{cc - RR_{oo}(1 - ccoos\,\alpha_{1nn} + \frac{\theta\theta_1}{2})}{cc}\varepsilon\varepsilon_{cc} \quad (4)$$

3- Compute the force of the whole concrete compression segment as if there is no void

$$CC_{cc1} = 4\,RR^2_{oo}\int_0^{\alpha\alpha_1} ssssnn^2\,\alpha_{1nn} + \frac{\theta\theta_1}{2}\sin\frac{\theta\theta_1}{2} * \sigma\sigma_{cc1nn} \quad (5)$$

4- Compute the concrete stress $\sigma\sigma_{cc1nn}$ using Yu et al. (2006) model (Fig. 10)

5- Compute the strain in each virtual strip segment inside the void as if there is a concrete infill

$$\varepsilon_{cc2nn} = \frac{c - (RR_{oo} - RR_{ii}\cos\alpha_{2nn} + \frac{\theta\theta_2}{2})}{cc}\varepsilon_{cc} \quad (6)$$

6- Compute the force of the virtual strip segment inside the void

$$CC_{cc2} = 4\,RR_{ii}^2 \int_0^{\alpha\alpha_2} sssnn^2\,\alpha_{2nn} + \frac{\upsilon\upsilon_2}{2}\sin\frac{\upsilon\upsilon_2}{2} * \sigma_{cc2nn} \quad (7)$$

7- Compute the concrete stress σ_{cc2nn} using Yu et al. (2006) model (Fig. 10)

8- Subtract CC_{CC2} from CC_{CC1} to get the actual compression force in the concrete shell (CC_{CC})

$$CC_{CC} = 4\left(RR_{OO}^2 \int_0^{\alpha\alpha_1} sssnn^2\,\alpha_{1nn} + \frac{\upsilon\upsilon_1}{2}\sin\frac{\upsilon\upsilon_1}{2} * \sigma_{cc1nn} - RR_{ii}^2 \int_0^{\alpha\alpha_2} sssnn^2\,\alpha_{2nn} + \frac{\upsilon\upsilon_2}{2}\sin\frac{\upsilon\upsilon_2}{2} * \sigma_{cc2nn}\right) \quad (8)$$

9- Compute the compressive force of each segment of steel tube

$$CC_{sscnn} = 2\int_0^{\alpha\alpha_2} tt_{ss} * RR_{ii} * \frac{\theta_2}{nn} * \frac{c - (RR_{oo} - RR_{ii}\cos\alpha_{2nn} + \frac{\theta\theta_2}{2})}{cc}\varepsilon_{cc} * EE_{ss} \quad (9)$$

where tt_{ss} and EE_{ss} are the thickness and the Young's modulus of the steel tube

10- Compute the tensile force of each segment of steel tube

$$TT_{ssssnn} = 2\int_0^{\alpha\alpha_3} tt_{ss} * RR_{ii} * \frac{\theta\theta_3}{nn} * \frac{(RR_{oo} - cc) + RR_{ii}\cos\alpha_{3nn} + \frac{\theta\theta_3}{2}}{cc}\varepsilon_{cc} * EE_{ss} \quad (10)$$

11- After attending the force equilibrium ($\Sigma\Sigma FF_{xx} = 0$), compute the bending moment

$$MM_{eexxss} = \int_0^{\alpha\alpha_1} CC_{cc1nn} * RR_{oo} * \cos\alpha_{1nn} + \frac{\theta\theta_1}{2} - \int_0^{\alpha\alpha_2} CC_{cc2nn} * RR_{ii} * \cos\alpha_{2nn} + \frac{\theta\theta_2}{2} + \int_0^{\alpha\alpha_2} CC_{sscnn} * RR_{ii} * \cos\alpha_{2nn} + \frac{\theta\theta_2}{2} + \int_0^{\alpha\alpha_3} TT_{ssssnn} * RR_{ii} * \cos\alpha_{3nn} + \frac{\theta\theta_3}{2} \quad (11)$$

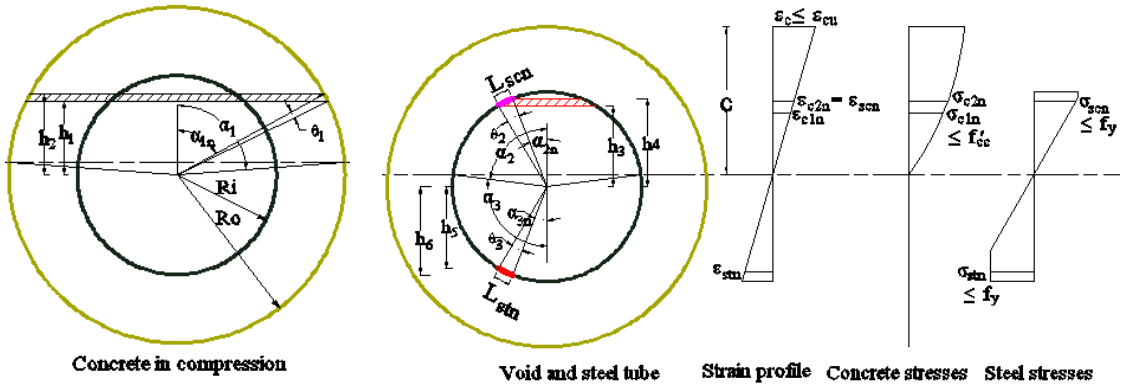

Figure 10 — Cross-sectional analysis

CONCLUSION

This paper presents the experimental results of hollow-core fiber-reinforced polymer concrete steel (HC-FCS) precast column. The precast HC-FCS column consists of a concrete shell sandwiched between an outer fiber-reinforced polymer (FRP) tube and an inner steel tube. The column had an outer diameter of 610 mm (24 inches) while the steel tube had a diameter of 406 mm (16 inches). The shear span-to-depth ratio of the column was 4.0. The steel tube of the column was embedded into a reinforced concrete footing with an embedded length of 1.6 times the steel tube diameter, while the FRP tube was truncated at the top surface of the footing face, i.e., the FRP tube confined the concrete shell only. The column had a steel tube embedment length of 635 mm (25 inches) into the footing. The column was originally tested under constant axial load and lateral cyclic load. Due to the insuffecient embeddment length, pullout failure and footing damage was observed. In the current study, the column was inserted into a newly constructed footing using the same embbedment length but with a corrugated steel pipe (CSP) that was inserted into the footing to improve the pullout performance of the column.

The column with CSP did not suffer severe visual damage into the footing. Furthermore, the column displayed lateral drift of 14.5% in the pushing direction and the test was terminated due to FRP rupture while it was terminated at the pulling direction due to the actuator reached its ultimate displacement without any visual damage to the column. The

original column without CSP displayed a lateral drift of 11.6% and the test was terminated due to the steel tube pullout failure.
Using the CSP into the footing was able to trigger the plastic capacity of the column with yielding of the steel tube. The flexural beam theory underpredicted the flexural strengths of the test specimens by 17% and 10.7% for columns without and with the CSP , respectively.

ACKNOWLEDGEMENT

Missouri University of Science and Technology conducted this research with funding provided by Missouri Department of Transportation (MoDOT). Gratefully, contribution from ATLAS Tube is appreciated. Discounts on FRP tubes from Grace Composites and FRP Bridge Drain Pipe are also appreciated. However, any opinions, findings, conclusions, and recommendations presented in this paper are those of the authors and do not necessarily reflect the views of the sponsors.

REFERENCES

1. Tran, H.V., *Drilled shaft socket connections for precast columns in seismic regions*. 2015, Universityof Washington.
2. Dawood, H., M. Elgawady, and J. Hewes, *Factors affecting the seismic behavior of segmental precast bridge columns.* Frontiers of Structural and Civil Engineering, 2014. **8**(4): p. 388-398.
3. Ozbakkaloglu, T. and B.L. Fanggi, *Axial compressive behavior of FRP-concrete-steel double-skin tubular columns made of normal-and high-strength concrete.* Journal of Composites for Construction, 2013.
4. Ozbakkaloglu, T. and Y. Idris, *Seismic behavior of FRP-high-strength concrete–steel double-skin tubular columns.* Journal of Structural Engineering, 2014.
5. Ozbakkaloglu, T. and B.A.L. Fanggi, *FRP–HSC–steel composite columns: behavior under monotonic and cyclic axial compression.* Materials and Structures, 2013. **48**(4): p. 1075-1093.
6. Shakir-Khalil, H., *Composite columns of double-skinned shells.* Journal of Constructional Steel Research, 1991. **19**(2): p. 133-152.
7. Teng, J. and L. Lam, *Behavior and modeling of fiber reinforced polymer-confined concrete.* Journal of structural engineering, 2004. **130**(11): p. 1713-1723.
8. Ozbakkaloglu, T. and E. Akin, *Behavior of FRP-confined normal-and high-strength concrete under cyclic axial compression.* Journal of Composites for Construction, 2011. **16**(4): p. 451-463.
9. Abdelkarim, O.I. and M.A. ElGawady, *Behavior of hollow FRP–concrete–steel columns under static cyclic axial compressive loading.* Engineering Structures, 2016. **123**: p. 77-88.
10. Anumolu, S., O.I. Abdelkarim, and M.A. ElGawady, *Behavior of Hollow-Core Steel-Concrete-Steel Columns Subjected to Torsion Loading.* Journal of Bridge Engineering, 2016: p. 04016070.
11. Han, Lin-Hai, Zhong Tao, Hong Huang, and Xiao-Ling Zhao , *Concrete-filled double skin (SHS outer and CHS inner) steel tubular beam-columns.* Thin-walled structures, 2004. **42**(9): p. 1329-1355.
12. Albitar, M., T. Ozbakkaloglu, and B.A.L. Fanggi, *Behavior of FRP-HSC-steel double-skin tubular columns under cyclic axial compression.* Journal of Composites for Construction, 2014.
13. Idris, Y. and T. Ozbakkaloglu, *Flexural behavior of FRP-HSC-steel double skin tubular beams under reversed-cyclic loading.* Thin-Walled Structures, 2015. **87**: p. 89-101.
14. Idris, Y. and T. Ozbakkaloglu, *Seismic behavior of high-strength concrete-filled FRP tube columns.* Journal of Composites for Construction, 2013.
15. Abdelkarim, O. I., ElGawady, Mohamed A., Gheni, Ahmed, Anumolu, Sujith, Abdulazeez, M. M., , *Seismic Performance of Innovative Hollow-Core FRP–Concrete–Steel Bridge Columns.* Journal of Bridge Engineering, 2016: p. 04016120.16.
16. Abdelkarim, O.I. and M.A. ElGawady, *Analytical and finite-element modeling of FRP-concrete-steel double-skin tubular columns.* Journal of Bridge Engineering, 2014. **20**(8): p. B4014005.
17. Abdelkarim, Omar I., Ahmed Gheni, Sujith Anumolu, and Mohamed A. ElGawady. *Seismic behavior of hollow-core FRP-concrete-steel bridge columns*. in *Structures Congress 2015*. 2015.
18. Abdulazeez, M.M. and M.A. ElGawady, *Seismic Behavior of Precast Hollow-Core FRP-Concrete-Steel Column having Socket Connection.* Proc., Transportation Research Board (TRB) 96th Annual Meeting, Transportation Research Board.

19. Abdelkarim, O.I. and M.A. ElGawady, *Performance of hollow-core FRP–concrete–steel bridge columns subjected to vehicle collision.* Engineering Structures, 2016. **123**: p. 517-531.
20. Grauvilardell, Jorge E., Daeyong Lee, Jerome F. Hajjar, and Robert J. Dexter., *Synthesis of Design, Testing, and Analysis Research on Steel Column Base Plate Connections in High-seismic Zones*. 2005.
21. Hitaka, T., K. Suita, and M. Kato. *CFT Column base design and practice in Japan*. in *Proceedings of the International Workshop on Steel and Concrete Composite Construction*. 2003. Citeseer.
22. Marson, J. and M. Bruneau, *Cyclic testing of concrete-filled circular steel bridge piers having encased fixed-based detail.* Journal of Bridge Engineering, 2004. **9**(1): p. 14-23.
23. Morino, S., J. Kawaguchi, A. Tsuji, and H. Kadoya., *Strength and stiffness of CFT semi-embedded type column base.* Proceedings of ASSCCA, 2003.
24. Roeder, C.W. and D.E. Lehman. *An economical and efficient foundation connection for concrete filled steel tube piers and columns*. in *International conference on composite construction in steel and concrete*. 2008.
25. Kingsley, A., *Experimental and analytical investigation of embedded column base connections for concrete filled high strength steel tubes*, in *Univ. of Washington*. 2005, Univ. of Washington: Seattle, WA.
26. Lee, J.R., *Experimental Investigation of Embedded Connections for Concrete-filled Steel Tube Columns Subjected to Combined Axial-flexural Loading*. 2011, University of Washington.
27. Williams, T.S., *Experimental investigation of high strength concrete filled steel tubes in embedded column base foundation connections*. a thesis submitted in partial fulfillment of the degree of Master of Science in Civil Engineering, University of Washington, Seattle, WA.2006.
28. Abdelkarim, O. I., Gheni, A., Anumolu, S., and ElGawady, M. A., *Hollow-Core FRP-Concrete-Steel Bridge Columns Under Extreme Loading*. No. cmr 15-008. 2015.
29. Yu, T., Y. L. Wong, J. G. Teng, S. L. Dong, and E. S. Lam. , *Flexural behavior of hybrid FRP-concrete-steel double-skin tubular members.* Journal of Composites for Construction, 2006. **10**(5): p. 443-452.
30. Caltrans, S., *Caltrans seismic design criteria, v. 1.7*. 2013, April.
31. Imbsen, R.A., *AASHTO guide specifications for LRFD seismic bridge design.* American Association of State Highway & Transport Officials, Subcommittee for seismic effects on bridges, 2007.
32. AASHTO. *AASHTO-LRFD Bridge Design Specifications* – Customary US Units, sixth edition, Washington, DC, 2012